SF2A 2012
S. Boissier, P. de Laverny, N. Nardetto, R. Samadi, D. Valls-Gabaud and H. Wozniak (eds)

THE EXTRAORDINARY CLUSTER OF GALAXIES ABELL 3376: AN OPTICAL VIEW

F. Durret[1], C. Perrot[2], G. B. Lima Neto[3], C. Adami[4] and J. Bagchi[5]

Abstract. Abell 3376 is a merging cluster of galaxies at redshift $z = 0.046$. It is famous mostly for its giant radio arcs, and shows an elongated and highly substructured X-ray emission, but has not been analysed in great detail at optical wavelengths. We have obtained deep images of Abell 3376 in the B and R bands and present here preliminary results on the B band galaxy luminosity function.

Keywords: Galaxies: clusters: individual: Abell 3376, Galaxies: luminosity function, mass function

1 Introduction

Abell 3376[i] is a merging cluster of galaxies at redshift $z = 0.046$. Its most remarkable feature is the existence of giant ($\sim$2 Mpc $\times$ 1.6 Mpc) ring-shaped nonthermal radio-emitting structures discovered by Bagchi et al. (2006, see their Fig. 1). These structures can be naturally explained by the acceleration of electrons due to the merger of two clusters.

The fact that it is a merging structure is indeed confirmed in X-rays. The XMM-Newton image of Abell 3376 is strongly elongated along the northeast-southwest axis joining the two giant radio arcs, and the temperature and metallicity maps of the X-ray gas show strong inhomogeneities (see Bagchi et al. 2006, Fig. 2). Recent numerical simulations by Machado & Lima Neto (2012) based on the parallel SPH code Gadget-2 have been able to reproduce the X-ray emissivity map, and suggest an approximately head-on collision with a mass ratio of about 3:1, observed about 0.2 Gyr after the instant of central passage, and taking place very close to the plane of the sky. Still another proof for merging resides in the fact that the brightest cluster galaxy is far from the region with strong X-ray emission, as seen in Fig. 1.

Note that Abell 3376 is part of the WINGS survey (Fasano et al. 2006) and its galaxy spatial distribution confirms the existence of substructures (Ramella et al. 2007). We retrieved from the NED data base a catalogue of galaxies with V band magnitudes within a radius of 40 arcmin around the cluster.

2 New optical data

We have obtained deep optical images in the B and R bands with the Cerro Tololo 4m telescope and the MOSAIC2 camera. Individual exposure times were 300 s in B and 2000 s in R. In total, we obtained 4 images in B and 4 images in R, in each of two adjacent regions covering the east and west parts of the cluster.

Since the cluster was observed during a single entire night, the airmass variations were important, so the images were extinction corrected individually after the usual bias and flat field corrections. They were then assembled into two large images, one in B and one in R, using the SCAMP and SWARP softwares developed by E. Bertin (`http://www.astromatic.net/`). These images cover $1.16065 \times 0.5947 = 0.69028$ deg^2 (scale 0.266 arcsec/pixel). Note that since the individual exposures in the R band were long, objects brighter than R$\sim$ 19 are saturated and will not be considered for scientific purposes.

[1] UPMC Université Paris 06, UMR 7095, Institut d'Astrophysique de Paris, 98bis Bd Arago, F-75014, Paris, France
[2] Observatoire de Paris-Meudon, France
[3] IAG, USP, R. do Matão 1226, 05508-090, São Paulo/SP, Brazil
[4] Aix Marseille Université, CNRS, LAM (Laboratoire d'Astrophysique de Marseille) UMR 7326, 13388, Marseille, France
[5] IUCAA, Pune University Campus, Post Bag 4, Pune 411007, India
[i] Based on observations taken with the CTIO Blanco and SOAR telescopes. This research has made use of the NED data base.

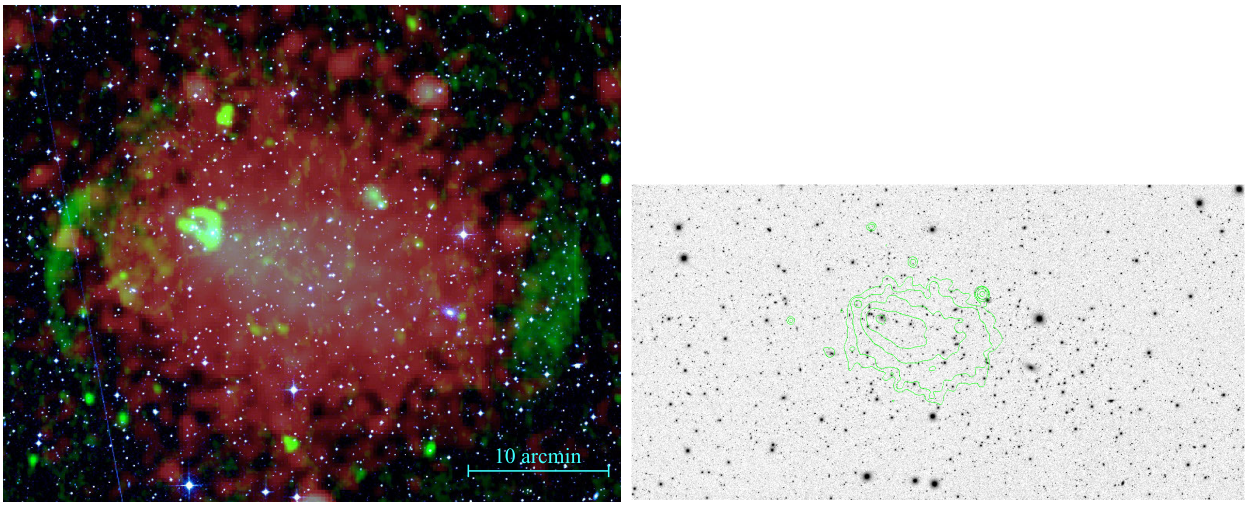

Fig. 1. Left: image of Abell 3376 with the radio (VLA, 1.4 GHz) and X-ray (XMM-Newton) emissions superimposed on the optical one, in green and red respectively. **Right:** optical image obtained with the CTIO/Blanco telescope with XMM-Newton X-ray contours superimposed. North is top and east to the left.

In order to obtain a photometric calibration of these images, since no standard stars had been taken, we reobserved the central region of Abell 3376 the following year with the SOAR telescope in the same bands. These images were taken in photometric conditions with respective exposure times of 600 s and 300 s in B and R, and covered a region of $0.084125 \times 0.08075 = 0.0067931$ deg^2 (scale 0.15 arcsec/pixel). We calibrated these images photometrically with Landolt standard stars, cross-identified objects present in the Blanco and SOAR images, and thus calibrated the Blanco images in B and R.

We now concentrate only on the deep large Blanco images.

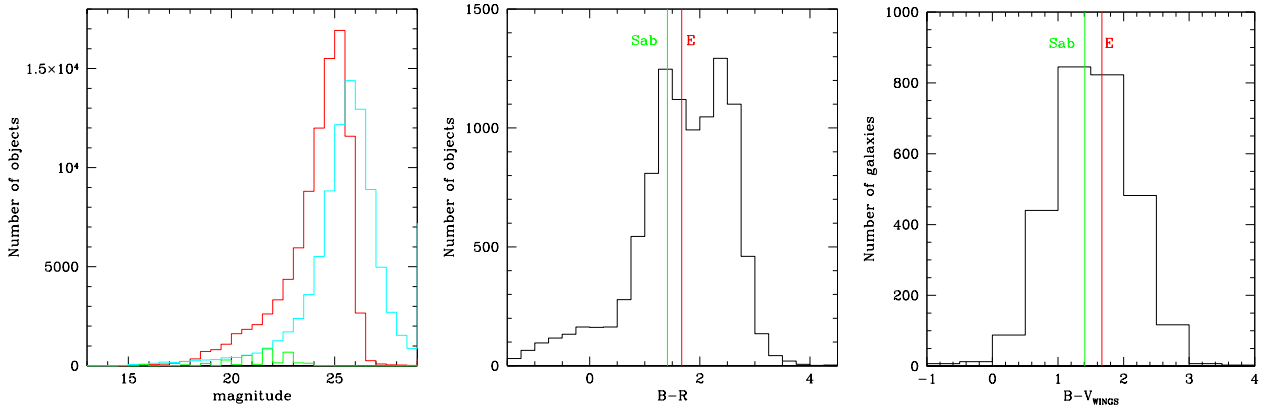

Fig. 2. Left: magnitude histograms for all the objects (stars+galaxies) detected in our images in the B (cyan) and R (red) bands. The green histogram shows the *galaxy* counts in the V band from the WINGS survey. **Middle:** (B-R) histogram, with typical values for elliptical and Sab galaxies indicated as red and green lines respectively (taken from Fukugita et al. 1995). **Right:** (B-V$_{WINGS}$) histogram, with typical values for elliptical and Sab galaxies indicated as red and green lines.

Magnitude histograms in the B and R bands, together with the (B-R) histogram are displayed in Fig. 2 for all the objects of our images (stars + galaxies). In order to confirm the quality of our photometric calibration, we also show in this figure the histogram of the (B-V$_{WINGS}$) colour.

The star-galaxy separation was based on the maximum surface brightness $\mu_{max,R}$ versus R band magnitude diagram.

3 The galaxy luminosity function in the B band

Two methods are usually applied to compute galaxy luminosity functions. The first one is to draw a colour-magnitude diagram, to superimpose on this diagram the positions of galaxies having a spectroscopic redshift in the cluster in order to define the position of the red sequence as well as possible, and to extract the galaxies belonging to the cluster along this red sequence. The second method is to count all the galaxies in magnitude bins and subtract statistically the contribution of background galaxies, using field galaxy counts.

In view of the saturation problems in the R band image, the first method cannot be applied, since we cannot define the red sequence for galaxies brighter than R∼19, which are those with spectroscopic redshifts. We shall therefore apply the second method, and subtract the field galaxy counts per square degree taken by McCracken et al. (2003) in the same filters.

Since more tests are necessary to test the quality of our R band data, we will present here only our results in the B band.

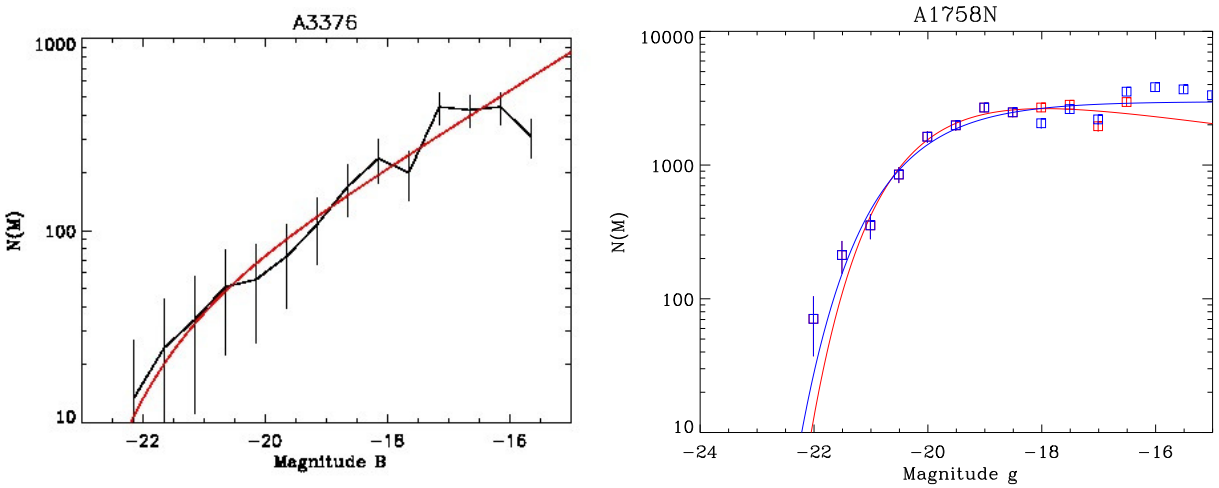

Fig. 3. Left: Galaxy luminosity function of Abell 3376 in the B band. **Right:** Galaxy luminosity function of the merging cluster Abell 1758 in the g band. The blue and red points correspond to the two methods to select galaxies described in the text, and the best Schechter function fits are drawn with the same colours as the corresponding points. At bright magnitudes the points exactly coincide, and because the blue points were plotted after the red ones, they appear blue.

The galaxy luminosity function in the B band (as a function of absolute magnitude, to make the comparison easier with other clusters, assuming a distance modulus of 36.40 for Abell 3376) is shown in Fig. 3. It was fit by a Schechter function:

$$S(M) = 0.4 \ln 10 \, \phi^* \, y^{\alpha+1} \, e^{-y}$$

with $y = 10^{0.4\,(M^*-M)}$.

The parameters of the Schechter function fit are $M^* = -20.59 \pm 0.23$ and $\alpha = -1.33 \pm 0.25$ in the $[-22.15, -15.65]$ B band absolute magnitude interval. Note that the faint end slope depends on the limit set at faint magnitudes.

In order to check down to which magnitude we could reasonably fit the GLF, we performed simple simulations to estimate the completeness of our galaxy catalogue as a function of magnitude. Our method is to add "artificial stars" (i.e. 2D Gaussian profiles with the same full-width-at-half-maximum as the average image point spread function) of different magnitudes to the CCD images and attempted to recover them by running SExtractor again with the same parameters used for object detection and classification on the original images. In this way, the completeness was measured on the original images.

These simulations give a completeness percentage for stars. This is obviously an upper limit for the completeness level for galaxies, because stars are easier to detect than galaxies. However, we have shown that this method yields a good estimate of the completeness for normal galaxies if we apply a shift of ~ 0.5 mag (see Adami et al. 2006). Results are shown in Fig. 4.

From these simulations, and taking into account the fact that the results are worse by ~ 0.5 mag for mean galaxy populations than for stars, we can consider that our galaxy catalogue in the B band is complete to better than 90% for B$\leq$ 24.5.

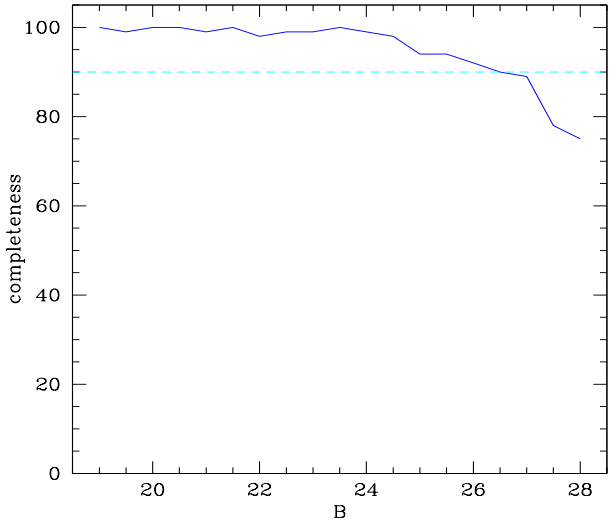

Fig. 4. Completeness as a function of magnitude in percentages in the B band for point–like objects. A shift of ~ 0.5 mag gives a good estimate of the completeness for galaxies (see text). The dashed line shows the 90% completeness level (for stars).

The faint end slope of the galaxy luminosity function has therefore been estimated in a magnitude interval where the completeness is still higher than 90%, and can therefore be considered as reliable.

4 Conclusions

The best fit parameters for the galaxy luminosity function in the B band for Abell 3376 can be compared to another merging cluster, Abell 1758 North, which we recently analysed using exactly the same method (Durret et al. 2011). We derived for this cluster a galaxy luminosity function in the g band and found a faint end slope $\alpha = -1.00 \pm 0.02$ (Durret et al. 2011). This slope is notably flatter than the one we estimated for Abell 3376, as clearly seen in Fig. 3.

An explanation could be that the mergers in these two clusters do not have the same age and that the faint end slope varies with time. We are in the process of analysing galaxy luminosity functions in a sample of clusters at redshifts up to 0.9 in all stages of merging, from relaxed to strongly substructured. This should shed light on the influence of mergers on the galaxy distributions in clusters.

We thank Emmanuel Bertin for his help and advice on his software. We acknowledge financial support from CNES and CAPES/COFECUB program 711/11.

References

Bagchi J., Durret F., Lima Neto G.B., Paul S. 2006, Science 314, 791

Durret F., Laganá T., Haider M. 2011, A&A 529, 38

Fasano G., Marmo C., Varela J. et al. 2006, A&A 445, 805

Fukugita M., Shimasaku, K., Ichikawa T. 1995, PASP 107, 945

Machado R.E.G. & Lima Neto G.B. 2012, arXiv:1209.0632

McCracken H.J., Radovich M., Bertin E. et al. 2003, A&A 410, 17

Ramella M., Biviano A., Pisani A. et al. 2007, A&A 470, 39